TiO$_2$/BaTiO$_3$-assisted photocatalytic mineralization of diclofop-methyl on UV-light irradiation in the presence of oxidizing agents

L. Gomathi Devi[*], G. Krishnamurthy

Department of Post Graduate Studies in Chemistry, Central College Campus, Dr. B.R. Ambedkar Veedi, Bangalore University, Bangalore 560001, India

ARTICLE INFO

ABSTRACT

Gas chromatograph–mass spectroscopic identification of intermediate products in the degradation of diclofop-methyl and the kinetics of the reaction has been investigated. Formation of 4-[(2,4-dichlorophenoxy) phenoxy] ethane and (2,4-dichlorophenoxy) phenol was investigated. The other intermediate products are 2,4-dichlorophenol, 2,4-dichlorobenzene, phenol and acetic acid have been ascertained. The decrease in the concentration of the parent/intermediate compounds is followed by UV–vis spectral study and the supportive information on the functional groups in the intermediates has been obtained from IR-spectroscopy. Degradation process proceeds with oxidation–reduction reaction by the attack of OH$^\bullet$, H$^\bullet$, O$_2^{\bullet-}$ free radicals, which are photogenerated on the UV-light illuminated TiO$_2$/BaTiO$_3$ photocatalysts particles in aqueous medium. In this presentation another wide band gap semiconductor BaTiO$_3$ is shown to have comparable photocatalytic efficiency. The oxidizing agents are added to accelerate the rate of the reaction by enhancing the formation of free radicals. Based on the intermediates formed in the process of degradation, a suitable mechanism has been proposed.

© 2008 Elsevier B.V. All rights reserved.

1. Introduction

The contamination of surface water with herbicides results primarily from surface run off from agricultural activities. Pesticides constitute the large group of polluting chemicals. The industrial waste is another major source for pesticide contamination. Post application and seasonal concentrations of different herbicides have been reported to exceed the maximum contaminant level permitted for surface waters [1,2]. In this regard diclofop-methyl (DCM) is a post emergence herbicide used to control wild oats and annual grassy weeds brassicas, carrots, peas, potatoes, field beans, French beans, broad beans, barley, wheat, parsnip, soya beans, oilseed rape, onions, sugar beet, lettuce, linseed oil and lucerne [3]. It has been reported that diclofop-methyl is one of the most commonly detected herbicide in many countries [2], with concentrations frequently reaching the milligrams per liter level due to its properties of persistence and mobility. This herbicide is toxic to many organisms and has low solubility in water. As a result, conventional biological remediation processes are not suitable to remove this pesticide from contaminated water and therefore alternative treatment methods are required. There are several treatment processes available for the destruction or detoxification of hazardous organic wastes because of the growing restrictions placed on waste discharges and land disposal. Amongst these methods the advanced oxidation process (AOP) are the most promising alternative to treat herbicide wastes [4,5] because, they involve the generation of hydroxyl radicals (HO$^\bullet$) that are species non-selective and highly reactive oxidants. The photocatalytic oxidation (PCO) of organic pollutants is based on the photochemical production of electron–hole pair in a solid semiconductor under irradiation by light of energy greater than its optical band. Photocatalytic oxidation involves two important aspects. First the adsorption of the pollutant on the surface of the photocatalyst takes place which is followed by oxidation with positively charged holes by direct abstraction of the pollutants electron. Second aspect is oxidation at the catalyst surface or in its vicinity with hydroxyl radicals.

Photocatalytic studies have usually employed titanium dioxide as the photocatalyst. The role of photocatalyst in general is to promote the reaction by lowering the activation energy. In this process it is essential to suppress the recombination process and to increase the life time of separated electron–hole pairs for the achievement of high photocatalytic activity, so that fast electron transfer occur from the surface of the catalyst to adsorbed intermediates. TiO$_2$ is the most commonly used photocatalyst in photocatalytic treatment of water and waste water because of its superior photo activity and low toxicity. In this presentation another wide band gap semiconducting particles BaTiO$_3$ is shown to have comparable photocatalytic efficiency. Photochemical activity of BaTiO$_3$ in aqueous

* Corresponding author. Tel.: +91 80 22961336.
E-mail address: gomatidevi_naik@yahoo.co.in (L. Gomathi Devi).

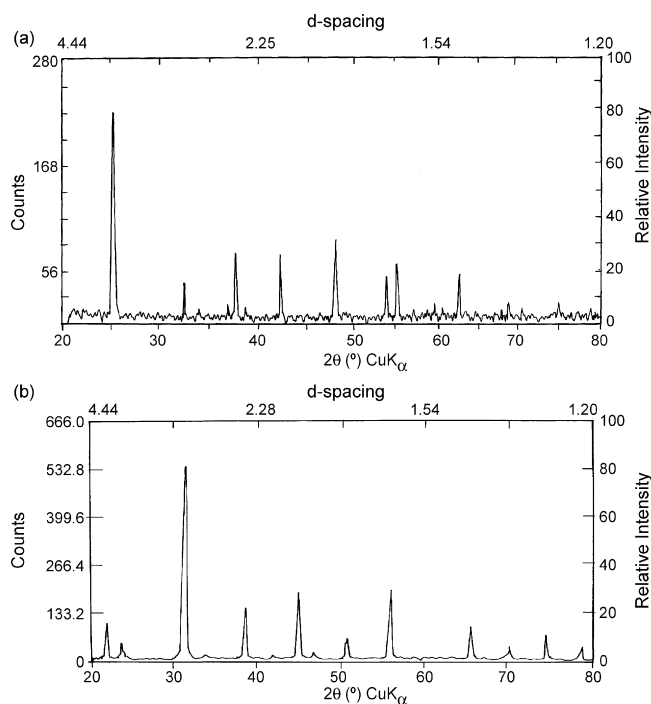**Fig. 1.** (a) XRD pattern for TiO_2 photocatalyst and (b) XRD pattern for $BaTiO_3$ photocatalyst.

solution under UV-light has been studied. This includes kinetic parameters like rate, rate constant, order and process efficiency. This work opens the possibility to develop more efficient photocatalysts for detoxification process. The aim of the present study is to investigate the prime mechanisms involved in the photocatalytic degradation of diclofop-methyl and to examine the effect of oxidizing agent and characterizing the intermediate products which are produced during the photo transformation process.

2. Experimental

2.1. Materials

2.1.1. Pesticide

The Pesticide sample of 96.6% pure was obtained from Rallis India Limited, an Agrochemical Research Center, Bangalore, India. The pesticide sample was used as such obtained from the industry. The pesticide diclofop-methyl: methyl 2-[4-(2,4-dichlorophenoxy) phenoxy] propionate is also called by the trade names Illoxan, Hoelon, Hoe-Gross, etc. It is a colorless, odorless crystals having molecular formula: $C_{16}H_{14}Cl_2O_4$; molecular weight: 341.20; melting point: 39–41 °C; boiling point: 173–175 °C at 0.1 mbar; vapor pressure: 3.4×10^{-7} mbar at 20 °C and 1.5×10^{-5} mbar at 30 °C. It is readily soluble in common organic solvents, e.g. acetone-40, xylene-50, methanol-40 (all in g/100 ml), etc., least soluble in water, i.e. only about 50 mg/l at 22 °C [3]. The structural formula of the herbicide is shown in Scheme 1.
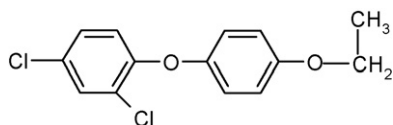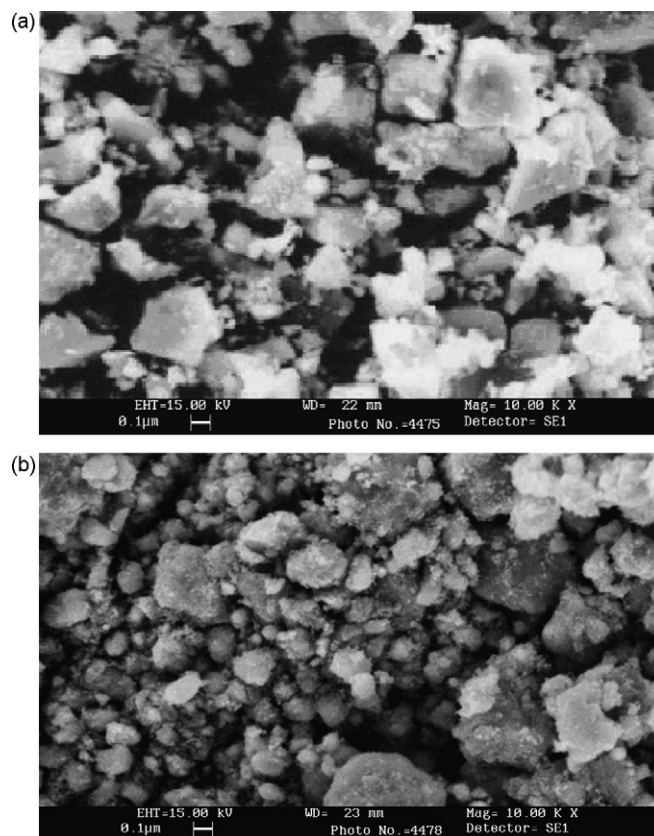

Scheme 1. Structure of diclofop-methyl.

Fig. 2. (a) SEM picture for TiO_2 powder and (b) SEM picture for $BaTiO_3$ powder.

2.1.2. TiO_2 and $BaTiO_3$

Titanium tetrachloride, ammonium hydroxide, Sulphuric acid and barium hydroxide, ammonium persulphate, hydrogen peroxide, nitric acid and sodium hydroxide all obtained from E-Merck chemicals. The solutions are prepared using double distilled water. The photocatalysts used are fine grained powders of anatase form of TiO_2 prepared by gel to crystalline conversion method to yield nanoparticles as reported earlier [6]. $BaTiO_3$ is also obtained by reaction of gels of hydrated titania with barium hydroxide as reported by Kutty and coworker [7]. The recovered solids from both the process were oven dried at 105–120 °C. $BaTiO_3$ is further annealed at 450 °C for 4 h and TiO_2 is annealed at 600 °C for 4 h.

2.2. Characterization of TiO_2 and $BaTiO_3$

The X-ray diffractograms for the finely ground $TiO_2/BaTiO_3$ photocatalyst powders are obtained using Phillips PW 1050/70/76 X-ray diffractometer which is operated at 30 kV and 20 mA. Cu Kα radiation was used with nickel filter. The scanning range employed was $2\theta = 5$–85°. The normal scanning speed was 2°/min and the check speed being 2 mm/min. The crystallite size measured from Scherrer's equation [8] relating the pure diffraction breadth (half-band width) to crystallite size normal to plane hkl as

$$D_{hkl} = \frac{K\lambda}{\beta \cos \theta} \tag{1}$$

where D_{hkl} is mean dimension in Å, λ is the wave length, β is the pure diffraction line broadening, θ is the Bragg's angle of the reflection h,k,l and K is the constant approximately equal to unity. Half bandwidth depends on crystallite size and microstrain in the lattice [9]. The calculated crystallite size of anatase TiO_2 is 17.93 nm and that of $BaTiO_3$ is 19.24 nm (Fig. 1a and b). The particle size

is obtained by SEM analysis of the samples using JEOL (JSM-840 A) scanning electron microscope. In SEM analysis the sample was dusted on aluminum and coated with a thin film of gold to prevent surface charging and to protect the material from thermal damage by electron beam. A uniform film thickness of about 0.1 mm was maintained for all samples. A linear intercept method is used to determine the particle size of the sample by image transfer analysis and further calculation is done on the computer. The average particle size for TiO$_2$ as obtained from the SEM analysis is 57–251 nm and that for BaTiO$_3$ is 85–286 nm (Fig. 2a and b).
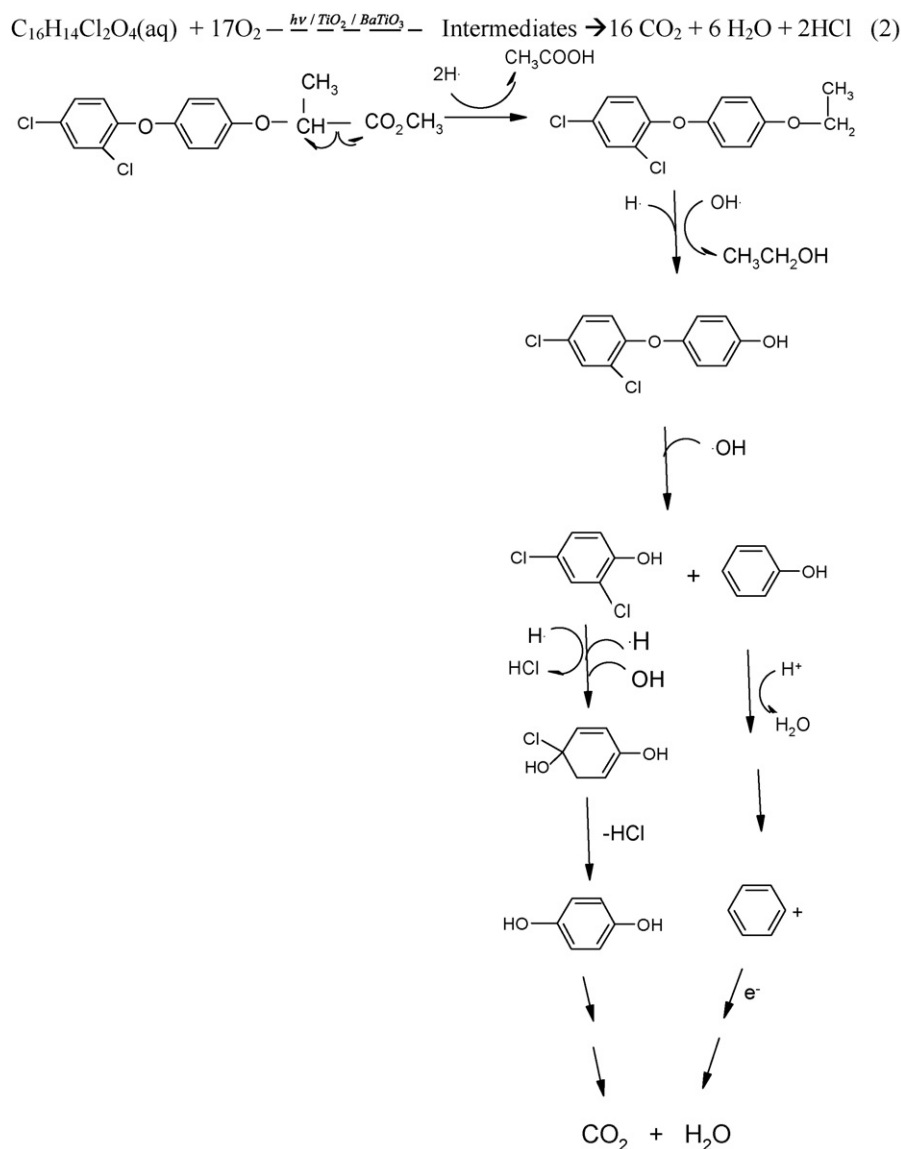
The diffused reflectance spectrum of anatase TiO$_2$ powder reveals the λ_{max} for TiO$_2$ at 413 nm, which corresponds to a band gap of 3.0 eV as calculated (Fig. 3) and that of BaTiO$_3$ shows at 372 nm and the calculated band gap is 3.33 eV (Fig. 4). The energy dispersive X-ray (EDX) analysis has been done using JSM-840A EDX analyzer. The result shows the perfect matching of atom percentage composition of TiO$_2$ and BaTiO$_3$ which is summarized in Table 1.

NOVA-1000 high gas sorption analyzer (Quanta chrome corporation, USA) version 3.70 is used to determine the surface area and pore volume. The adsorption/desorption tolerance was

Table 1
Collective results of characterization of TiO$_2$ and BaTiO$_3$ photocatalyst powders

Analysis	TiO$_2$	BaTiO$_3$
Atom % by EDX	Ti/O-33.25/66.75	Ba/Ti/O-19.63/20.25/60.12
Crystallite size by XRD (nm)	17.531	19.243
Particle size by SEM (nm)	57–251	85–286
Surface area by BET method (m^2/g)	50.536	34.141
Pore volume by BET (cc/g)	0.1859	0.0896

0.1000 mm Hg. The N$_2$ gas is used as adsorbate at the pressure $P_0 = 697.83$ mm Hg and bath temperature = 77.40 K. The weight and the density of TiO$_2$ sample used for the analysis are 0.1655 g (volume is 0.1528 cc) and 1.0420 g/cc and those for BaTiO$_3$ are 0.2825 g (volume is 0.2174 cc) and 1.2995 g/cc, respectively. The average pore diameter is found to be 147.179 Å and the surface area obtained is 8.4143 m^2 and the specific surface area is 50.539 m^2/g for TiO$_2$. The average pore diameter for BaTiO$_3$ is 104.953 Å and the surface area obtained is 9.6450 m^2 and the specific surface area is 34.1414 m^2/g. The details are presented in Table 1.

$$C_{16}H_{14}Cl_2O_4(aq) + 17O_2 \xrightarrow{h\nu\,/\,TiO_2\,/\,BaTiO_3} \text{Intermediates} \rightarrow 16\,CO_2 + 6\,H_2O + 2HCl \quad (2)$$

Scheme 2. Proposed reaction mechanism for the degradation of diclofop-methyl.

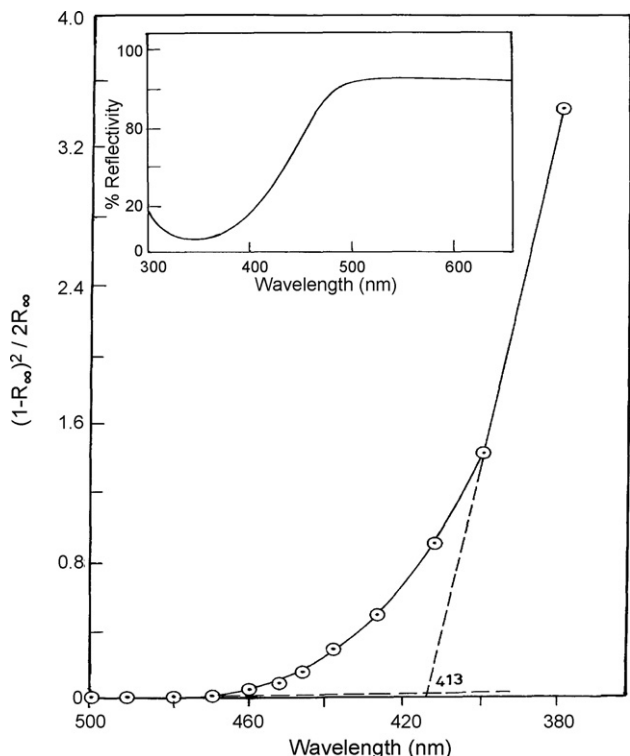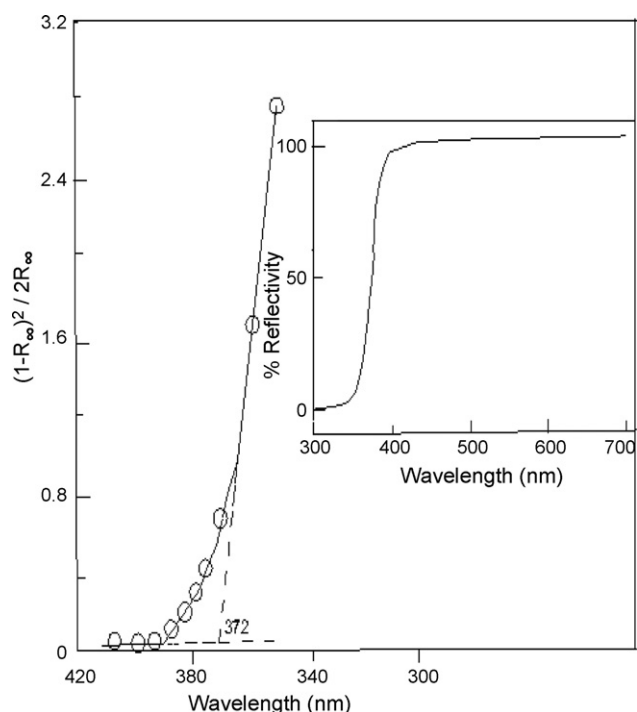**Fig. 3.** The plot of relative reflective intensity $(1 - R_\infty)^2/2R_\infty$ vs. wavelength with an inset figure of diffuse reflectance spectra of TiO$_2$.

Fig. 4. The plot of relative reflective intensity $(1 - R_\infty)^2/2R_\infty$ vs. wavelength with an inset figure of diffuse reflectance spectra of BaTiO$_3$.

2.3. Photoreactor and light source

The degradation experiments are carried out in a reaction cell of circumference −34 cm of 1 l capacity with the exposure area of 92.0378 cm^2. The light source is medium pressure 125 W mercury

vapor lamp whose wavelength peaks around 350–400 nm. The photon flux is found to be 7.75 mW/cm^2 as determined by ferrioxalate actionometry. The photoreaction experiments were performed by direct exposure into the reaction mixture. The experiments were performed at room temperature. The distance between the photoreactor and the lamp housing is 29 cm.

2.4. Photocatalytic degradation procedure

Photocatalytic degradation of DCM has been carried out under UV-light in the presence of TiO$_2$/BaTiO$_3$ catalyst suspensions. 10 ppm solution of DCM containing 300 mg of catalyst in suspension was made up to 400 ml is used. The reaction solution in all the experiments is stirred for 5–10 min before the start of illumination to facilitate the initial adsorption. The rate of stirring of the reaction solution was kept at 120 rpm. The temperature was normally maintained around 25 °C. A series of photodegradation experiments under different reaction conditions are performed. The photoreactor consists of an open glass vessel so as to allow the sample to be in contact with atmospheric air. Samples were withdrawn at different intervals of time to analyze the residual concentration and the intermediate formed during the process of degradation by various spectroscopic methods and they were centrifuged to remove suspended TiO$_2$/BaTiO$_3$ particles completely. The amount of DCM remaining at any given time is determined by using standard calibration curves from UV–vis spectrophotometer from the adsorption values.

3. Results and discussion

3.1. Aqueous systems in dark condition

Degradation of DCM in the absence of photocatalyst (TiO$_2$/BaTiO$_3$)/oxidizing agent/UV-light is negligible.

3.2. The kinetics of degradation of diclofop-methyl

The rate of degradation of DCM is expressed in terms of the residual concentration or the concentration of the substrate degraded as a function of time or the durations taken for the degradation of the pollutant. Fig. 5 is a plot of C/C_0 versus the degradation time,
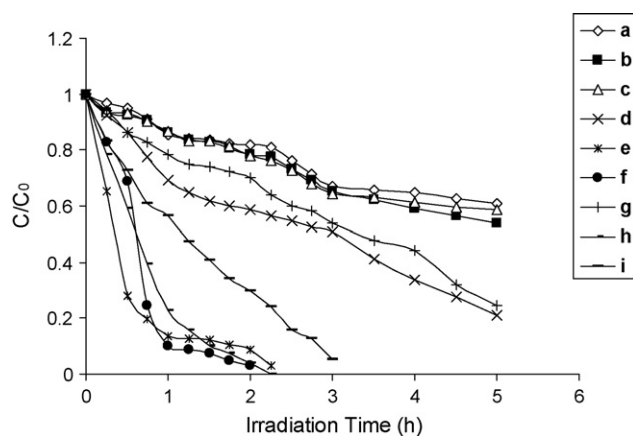

Fig. 5. Plot of C/C_0 vs. the degradation time, where C_0 is the initial concentration and C is the concentration at any instant of time. In the plot curves correspond to the experiments (a) only DCM in the absence of catalyst and oxidizing agents, (b) DCM with (NH$_4$)$_2$S$_2$O$_8$ and no catalyst, (c) DCM with H$_2$O$_2$ and no catalyst, (d) DCM with TiO$_2$ catalyst, (e) DCM with TiO$_2$ catalyst and (NH$_4$)$_2$S$_2$O$_8$, (f) DCM with TiO$_2$ catalyst and H$_2$O$_2$, (g) DCM with BaTiO$_3$ catalyst, (h) DCM with BaTiO$_3$ catalyst and (NH$_4$)$_2$S$_2$O$_8$, and (i) DCM with BaTiO$_3$ catalyst and H$_2$O$_2$.
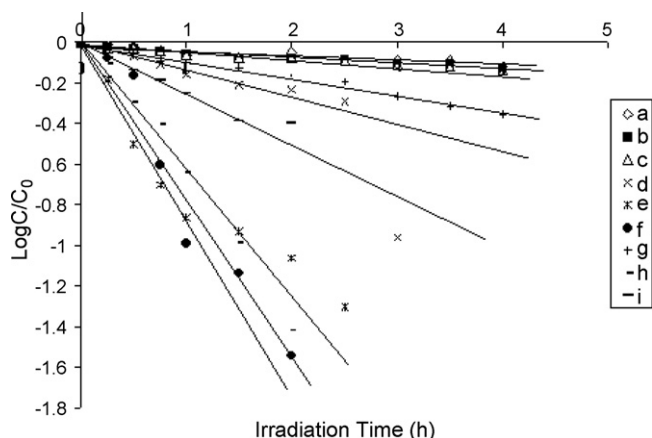
Fig. 6. Plot of log C/C_0 vs. irradiation time, which shows the dependency of the logarithm of residual concentration of DCM (negative values) on illumination. In the plot curves correspond to the experiments (a) only DCM in the absence of catalyst and oxidizing agents, (b) DCM with $(NH_4)_2S_2O_8$ and no catalyst, (c) DCM with H_2O_2 and no catalyst, (d) DCM with TiO_2 catalyst, (e) DCM with TiO_2 catalyst and $(NH_4)_2S_2O_8$, (f) DCM with TiO_2 catalyst and H_2O_2, (g) DCM with $BaTiO_3$ catalyst, (h) DCM with $BaTiO_3$ catalyst and $(NH_4)_2S_2O_8$, and (i) DCM with $BaTiO_3$ catalyst and H_2O_2.

where C_0 is the initial concentration and C is the concentration at any instant of time. The experiment in the absence of catalyst and oxidizing agent shows negligible degradation even after 5 h of irradiation. The degradation of DCM is around 8 h for both the catalysts in the absence of oxidizing agents. Destruction of herbicide with only $(NH_4)_2S_2O_8$ as an oxidizing agent and also with H_2O_2 is as shown in Fig. 5. High destructive rates are achieved in presence of both oxidizing agent and photo catalyst ($TiO_2/BaTiO_3$). The rate of degradation decreases in the presence of either oxidizing agent or catalyst alone when used. Photocatalyst along with oxidizing agent can lead to the better rates. This concept can be explained in the mechanism of heterogeneous photo catalysis. The electron hole pairs are generated on irradiation of semiconductor photo catalyst particle. If the recombination of these electron hole pairs takes place it represents a major energy-wasting step causing no degradation. Addition of an oxidizing agent avoids this recombination to some extent. Therefore addition of photo catalyst with an oxidizing agent shows pronounced effect on photo degradation. H_2O_2 and ammonium per sulphate acts as electron acceptors, when added to the reaction mixtures they enhance the formation of hydroxyl radicals causing faster oxidation of the pesticide molecule. Further involvement of these electron acceptors is to increase the oxidation rate of intermediate compounds. These oxidizing agents acting as electron acceptors increase the number of hydroxyl radicals which
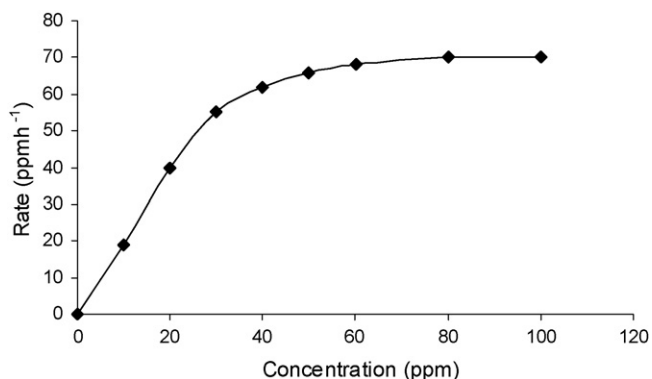
Fig. 7. Plot of velocity of degradation versus concentration of PM for the simple Langmuir-unimolecular reaction.
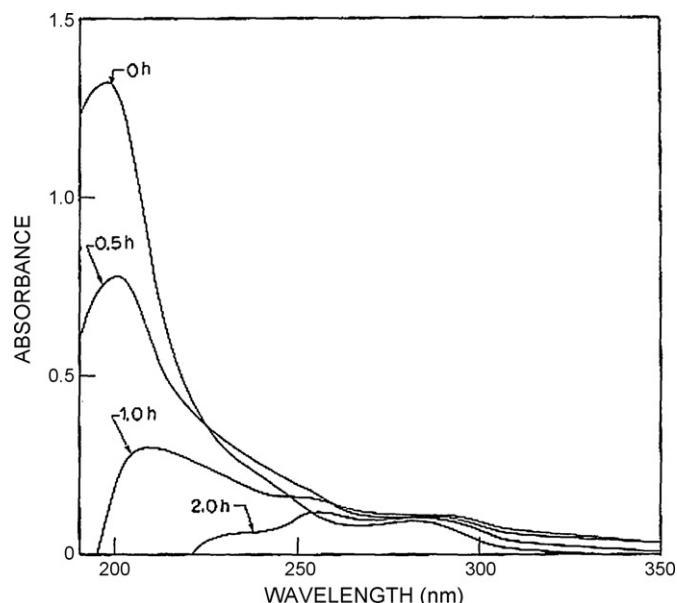
Fig. 8. UV–vis absorption spectra for the samples from the experiment with $BaTiO_3$ as the catalyst in the presence of APS (100 ppm) at different time at different time intervals (as indicated in the figure) for the degradation of 10 ppm of DCM.

are thought to be the primary oxidizing species. They are known to react very rapidly with organic molecules to yield hydroxylated radicals leading to subsequent reactions. These adduct radicals can lead to mineralization of organic molecules. In the absence of oxidizing agents both the photocatalysts show 30% degradation for 5 h of irradiation. Complete degradation takes place in 2.5 h with TiO_2 photocatalyst in the presence of either $(NH_4)S_2O_8$ or H_2O_2 (50 ppm). Comparitively $BaTiO_3$ shows a higher rate of degradation in the presence of $(NH_4)S_2O_8/H_2O_2$. This may be due to favorable coordinate environment of surface atoms, favorable red-ox properties of the oxide and appropriate oxidation state of the surface compared to TiO_2. The maximum rate values for TiO_2 with H_2O_2 and $(NH_4)S_2O_8$ are 1.758 and 1.494 h^{-1}, respectively. Similarly the rate values for $BaTiO_3$ are 1.87 and 1.08 h^{-1} respectively. Fig. 6 is plot of log C/C_0 versus irradiation time, which shows the dependency of the logarithm of residual concentration of DCM (negative values) on irradiation in the presence of catalyst and oxidant. The higher negative slopes of the lines show the faster rate of degradation. The rate constants are calculated using the corresponding slopes of the lines. The corresponding values are 1.5, 1.68, 1.92, 2.5, 8.15, 5.2, 0.81, 6.6 and 9.3 (all in 10^{-1}) per hour respectively.

3.2.1. Order of the degradation reaction

Order of the degradation reaction is determined by differential method. The velocity is measured at various values of the reactant concentration and a double logarithmic plot of velocity against the concentration shows the linear variation. The order obtained from this plot is 1.027 which approximates to first order.

3.2.2. Nature of adsorption

The plot of rate versus concentration (Fig. 7) describes the nature of adsorption. This plot shows first order rate in the beginning and this increases exponentially and the rate changes to zero-order at the saturation limit indicating clearly the Langmuir unimolecular adsorption reaction mechanism. The plot of the rate versus concentration is very much similar to the plot of fraction of surface covered versus concentration for Langmuir unimolecular adsorption mechanism [10].
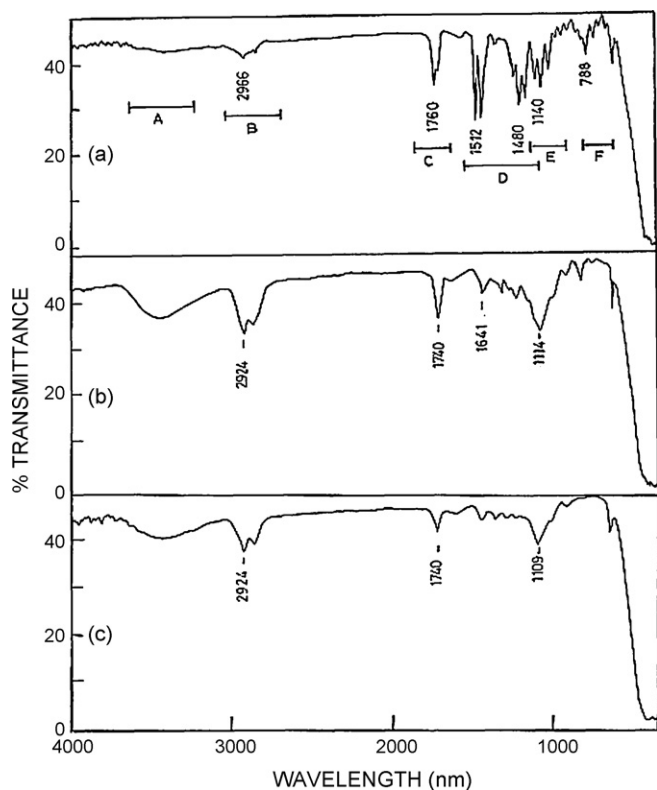
Fig. 9. The IR spectra for the samples of DCM (a) before irradiation, (b) after 0.5 h and (c) 1.0 h of irradiation from the experiment in the presence of catalyst and oxidizing agent.

3.3. Spectroscopic analysis

3.3.1. UV–vis spectral analysis

UV–vis spectrophotometer used for the photocatalytic degradation study is Shimadzu UV–vis-160 model. The aqueous samples were used for analysis in quartz cell of $1\,cm^2$ area. The concentrations during the degradation process are obtained from the calibration curve. The UV–vis absorption spectrum of sample of DCM before irradiation has three prominent characteristic absorption bands at 200, 240 and 285 nm. DCM is a substituted aromatic compound. The aromatic ring is expected to show the characteristic absorption bands at 184, 204 and 256 nm. In DCM these bands appear at 200 nm which is a characteristic peak of aromatic systems due to $\pi \to \pi^*$ transition (E-band), a weak band at 240 nm, is attributed to $\pi \to \pi^*$ transition (K-band) in aromatic/conjugated systems. In conjugated systems the energy separation between the ground and excited states is reduced and the system then absorbs at longer wavelengths with increasing intensity. The band at 285 nm, which is due to $n \to \pi^*$ transition (R-band) is attributed to chromophoric group >C=O in the diclofop methyl. In saturated aliphatic ketones, the $n \to \pi^*$ transition (around 280 nm) is the lowest energy transition. This $n \to \pi^*$ transition is forbidden by symmetry consideration. Thus the intensity of the band is low [11]. The band at 203 nm (λ_{max}) decreases in intensity on irradiation. This band is shifted to longer wavelength (210 nm) as shown in the absorption spectrum for the sample after 1 h of irradiation. This is a bathochromic shift due to the intermediate product formed during the degradation process. This band could be due to auxochrome –OH on the aromatic ring. At 0.25 h the band at 240 nm has disappeared and a new band at 255 nm appears. This could be due to the OH of phenolic compound formed during irradiation, which has been further supported by IR and GC–MS analysis. The band at
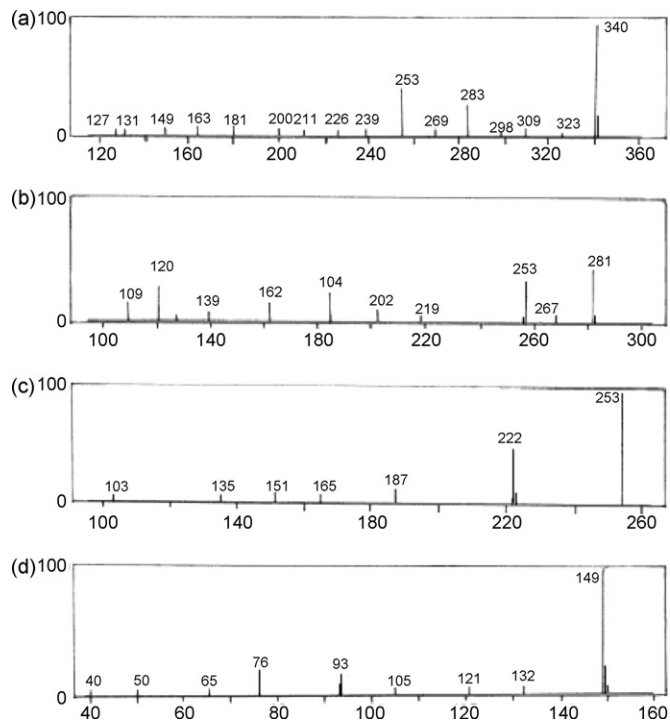
Fig. 10. GC–MS spectra of DCM: (a) the initial sample, (b) and (c) after 0.5 h of irradiation and (d) 1.0 h of irradiation.
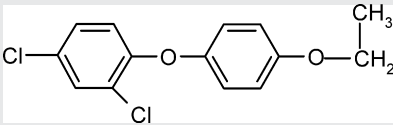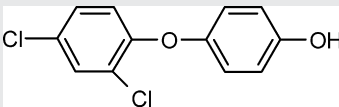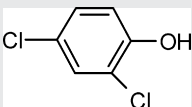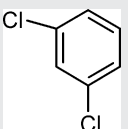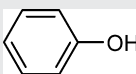
285 nm is slightly shifted to longer wavelength (bathochromic shift or red shift) and increases in intensity (hyperchromic effect). These changes are due to the presence of auxochrome (Fig. 8).

3.3.2. IR-spectral analysis

The IR spectral study is employed to follow up the degradation process and to identify the intermediate products. The IR spectrophotometer used was a Nicolet Impact 400 D FTIR. Sample for the best system in which the degradation reaction in presence of both photo catalyst and oxidizing agent is used for IR analysis. The samples were withdrawn at regular intervals, centrifuged and extracted into non-aqueous solvent petroleum ether (spectroscopic grade solvent) which is further dried by the addition of sodium sulphate and dried in a desiccator. Fig. 9 consists of spectra for the samples at different time intervals of irradiation. The initial spectrum taken at zero time of irradiation does not show any characteristic peak in the region 'A' (3400–3550 cm^{-1}), but the intermediate spectra shows a prominent broad peak in the region A, around 3500 cm^{-1} where N–H or O–H gives the characteristic strong peak. Since diclofop-methyl does not contain any N–H group it should be due to O–H of phenol, which arises only in the intermediate spectra. The other regions and corresponding groups are analyzed [11] in the following way: region B: for aromatic C–H stretch at 3008 cm^{-1} and methyl C–H stretch at 2966–2875 cm^{-1}, region C: for >C=O stretch at 1715 cm^{-1}, region D: for C···C ring stretch at 1600–1466 cm^{-1} [11]; region E: for C–O–C asymmetric stretching is at 1150–1085 cm^{-1}, C–H and C=C bending vibrations at 1000–500 cm^{-1}. region F: for C–Cl band. The spectrum (b) is for the sample taken after 0.5 h of irradiation in which many sharp peaks in the finger print region have disappeared. The substituted benzene ring, gives the peak in the region E. A broad band in the region around 3500 cm^{-1} appears which may correspond to O–H of the phenolic compound. In the spectrum (c) after 1 h of irradiation, the peak in the region 900–750 cm^{-1} has disappeared. This may be due to cleavage of C–Cl band. This information about the interme-

Table 2
The intermediate degradation products with ion mass identified from GC–MS analysis

Sl. no.	Ion mass	Intermediate product
1	(M$^+$-283)	
2	(M$^+$-252)	
3	(M$^+$-163)	
4	(M$^+$-149)	
5	(M$^+$-93)	

diates is further conformed by GC–MS analysis. The spectrum after 2 h of irradiation has the peaks of negligible intensities.

3.3.3. Gas chromatograph–mass spectroscopic analysis

GC–MS analysis has been carried out to confirm the intermediates formed during the degradation process. GC–MS spectral data is obtained on 17A Shimatzu gas chromatograph with QP-5050A mass spectrometer. The samples in the ether medium are injected in to the instrument in 0.1 μl quantity. The mass spectrum was obtained using electron impact ionization technique. The mass spectrum shows a peak at m/z value (M$^+$-340), which is the molecular ion peak (Fig. 10a) and the base peak at m/z value (M$^+$-253), which corresponds to 4-(2,4-dichlorophenoxy) phenol [12,13]. There are many smaller peaks for the fragment ions having the m/z values 325, 309, 298, 269, 239, 226, 211, 203, 181, 165, 149, 135 and 127 in the mass spectrum. In the GC spectrum after 0.5 h of irradiation has two major peaks having the m/z values (M$^+$-283) and (M$^+$-253), which corresponds to the intermediate molecular ions [4-(2,4-dichlorophenoxy) phenoxy] ethane and 4-(2,4-dichlorophenoxy) phenol respectively (Fig. 10b and c). The appearance of O–H peak in the IR spectrum also support for the formation of phenolic compound. The other intermediate products may be 2,4-dichlorophenol (M$^+$-163), phenol (M$^+$-93) and acetic acid. The mass spectrum after 1h of irradiation has the base peak at 149, which corresponds

to 2,4-dichlorobenzene (Fig. 10d). Table 2 gives the intermediate compounds and corresponding fragment ion masses. A probable reaction mechanism involving the above intermediates is proposed as shown in Scheme 2.

4. Conclusions

Photocatalytic degradation of diclofop-methyl is studied using the two photocatalysts TiO$_2$ and BaTiO$_3$ under UV-light illumination. BaTiO$_3$ is found to be more efficient than TiO$_2$ in the presence of ammonium persulphate. This may be due to favorable coordinate environment of surface atoms, favorable redox properties of the oxide and appropriate oxidation state of the surface compared to TiO$_2$. The complete mineralization of DCM has been observed within 2.0 h of illumination. The degradation of DCM follows the Langmuir-unimolecular kinetic model. The formation of [4-(2,4-dichlorophenoxy) phenoxy] ethane and 4-(2,4-dichlorophenoxy) phenol, 2,4-dichlorobenzene, etc., are identified as intermediates during the degradation process by GC–MS analysis with the support of UV–vis and IR spectral analysis. By observing the spectral changes that takes place during degradation and depending on the reaction conditions a suitable reaction mechanism has been proposed.

References

[1] I. Poulios, M. Kositzi, A. Kouras, Photocatalytic decomposition of trichlopyr over aqueous semiconductor suspensions, J. Photochem. Photobiol. A: Chem. 115 (1998) 175.
[2] J. Carla Garcia, K. Takashima, Photocatalytic degradation of imazaquin in an aqueous suspension of titanium dioxide, J. Photochem. Photobiol. A: Chem. 155 (2003) 215–222.
[3] A.M. Cummings, M.T. Ebron Mc Coy, J.M. Rogers, B.D. Barbee, Harris, Benzimidazole carbomate following exposure during early pregnancy, Fundam. Appl. Toxicol. 18 (10-5) (1992) 288–293.
[4] C.S. Turchi, D.F. Ollis, Photocatalytic degradation of organic water contaminants: mechanisms involving hydroxyl radical attack, J. Catal. 122 (1990) 178.
[5] K. Wang, J. Zhang, S. Yang, Y. Chen, UV or visible light induced photodegradation of AO7 on TiO$_2$ particles: the influence of anions, J. Photochem. Photobiol. A: Chem. 165 (2004) 201–207.
[6] L. Gomathi Devi, G.M. Krishnaiah, Photocatalytic degradation of *P*-amino-azobenzene and *P*-hydroxy-azobenzene using various heat treated TiO$_2$ as the photocatalyst, J. Photochem. Photobiol. A: Chem. 121 (1999) 141.
[7] P. Padmini, T.R.N. Kutty, Wet chemical synthesis of multicomponent hexaferrites by gel-crystallite conversion and their magnetic properties, J. Mater. Chem. 4 (12) (1994) 875.
[8] G.K. Williumson, W.H. Hall, X-ray line broadening from field aluminium and wolframite, Acta Met. 1 11 (1953) 22.
[9] A.R. West, Solid State Chemistry and its Applications, John Wiley and Sons Ltd., Singapore, 1984.
[10] K.J. Laidler, Chemical Kinetics, 2nd edn., Tata-McGraw Hill Publishing Co. Ltd., New Delhi, 1992.
[11] R.M. Silverstein, G.C. Bassler, T.C. Morrill, Spectroscopic Identification of Organic Compounds, 4th ed., John Wiley and Sons Inc., New York, 1981.
[12] N.E. Humbure, S.R. Kolbe, Herbicide Hand Book of the Weed Science Society of America, 6th ed., Weed Science Society of America, Champaign, IL, 1989.
[13] E.S. Brodsky, N.A. Klyuev, O.B. Smirnova, A.V. Dovgilievitz, I.I. Grandberg, GC–MS analysis of photodegradation products of diclofop-methyl, Int., J. Environ. Ann. Chem. 56 (1) (1994) 11–21.